



Manuscript ID:
IJRSEAS-2025-020510



Quick Response Code:



Website: <https://eesrd.us>



Creative Commons
(CC BY-NC-SA 4.0)

DOI: [10.5281/zenodo.17376608](https://doi.org/10.5281/zenodo.17376608)

DOI Link:
<https://doi.org/10.5281/zenodo.17376608>

Volume: 2

Issue: 5

Pp. 44-57

Month: October

Year: 2025

E-ISSN: 3066-0637

Submitted: 06 Sept. 2025

Revised: 11 Sept. 2025

Accepted: 06 Oct. 2025

Published: 31 Oct. 2025

Address for correspondence:

H. N. Dandgavhal, Ph.D Scholar,
Department of Electronics,
Mahatma Gandhi Vidyamandir's
Loknete Vyankatrao Hiray Arts,
Science and Commerce College,
Panchavati, Nashik, Affiliated to
Savitribai Phule Pune University,
Pune, Maharashtra, India
Email:
harshaldandgavhal.007@gmail.com

How to cite this article:

Dandgavhal, H. N., Patil, A. V.,
Patil, A. B., Shinde, U. P., &
Sayyad, S. B. (2025). SAR
Frequency Bands and Applications
for Environmental Monitoring and
Sustainable Earth Observation.
International Journal of Research
Studies on Environment, Earth, and
Allied Sciences, 2(5), 44–57.
<https://doi.org/10.5281/zenodo.17376608>

SAR Frequency Bands and Applications for Environmental Monitoring and Sustainable Earth Observation

H. N. Dandgavhal¹, Dr. U. P. Shinde², Dr. A. V. Patil³, Dr. S. B. Sayyad⁴,
Dr. A. B. Patil⁵

^{1,3,5}Ph.D Scholar, Department of Electronics, Mahatma Gandhi Vidyamandir's Loknete Vyankatrao Hiray Arts, Science and Commerce College, Panchavati, Nashik, Affiliated to Savitribai Phule Pune University, Pune, Maharashtra, India

²Professor, M. J. M. Arts, Commerce and Science College Karanjali Tal. Peth, Dist. Nashik, Maharashtra Affiliated to Savitribai Phule Pune University, Pune, Maharashtra, India

⁴Professor, MilliYA Art's, Science and Management Science College, Beed, Maharashtra Dr Babasaheb Ambedkar Marathwada University, Aurangabad, Maharashtra, India

Abstract

Synthetic Aperture Radar (SAR) has become a vital tool for Earth observation owing to its capability to capture data under all-weather and day-night conditions. The performance of SAR systems is strongly influenced by their operating frequency bands, each offering distinct penetration depths and scattering properties. This review highlights the applications of major SAR frequency bands—X, C, L, S, and P—in environmental monitoring and sustainable resource management. X-band is effective for high-resolution urban mapping and infrastructure monitoring, while C-band is widely applied in agriculture, soil moisture estimation, flood detection, and sea-ice studies. L-band enables deeper vegetation penetration, supporting biomass estimation, forest structure analysis, and soil roughness characterization. The upcoming S-band, as implemented in NASA-ISRO's NISAR mission, is expected to bridge soil and vegetation studies with balanced sensitivity. P-band, though less common, provides deeper canopy and subsurface insights, particularly valuable for biomass and geology. By comparing frequency-dependent applications, this paper underscores the potential of SAR in advancing sustainable environmental monitoring and climate resilience.

Keywords: Synthetic Aperture Radar (SAR); Frequency Bands (X, C, L, S, P); Sustainable Earth Observation; Soil Moisture and Agriculture.

Introduction

1. Electromagnetic Spectrum

Electromagnetic (EM) radiation is a fundamental physical phenomenon in which energy propagates through space or a material medium in the form of electromagnetic waves. These waves travel at the speed of light ($c \approx 3 \times 10^8$ m/s) in vacuum. An electromagnetic wave consists of two mutually perpendicular oscillating fields: the electric field (E) and the magnetic field (M). Both fields are orthogonal to each other and to the direction of propagation, thereby forming a transverse wave. This dual-field nature was predicted by Maxwell's equations and experimentally verified in various contexts [1].

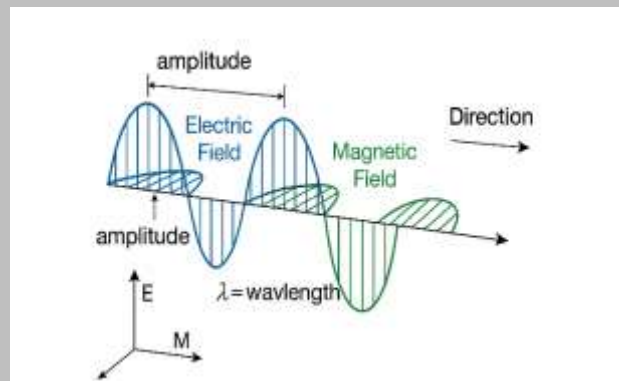


Figure 1.1 illustrates the direction of propagation of electromagnetic energy

Electromagnetic radiation is characterized by three interdependent properties: wavelength (λ), frequency (f), and speed (c). The relationship between these parameters is given by:

$$c = f \times \lambda \quad (1)$$

Where:

c = speed of light in vacuum (3×10^8 m/s)

f = frequency (Hz)

λ = wavelength (m)

The quantum nature of electromagnetic radiation is expressed through the Planck–Einstein relation, which defines the energy (E) of a photon:

$$E = h \times f = (h \times c) / \lambda \quad (2)$$

Where:

h = Planck's constant (6.626×10^{-34} J·s)

f = frequency (Hz)

λ = wavelength (m)

2. Electromagnetic Spectrum

The electromagnetic spectrum encompasses the complete range of electromagnetic radiation, spanning from low-frequency, long-wavelength radio waves to extremely high-frequency, short-wavelength gamma rays [2]. The spectrum is typically divided into regions based on wavelength and frequency ranges:

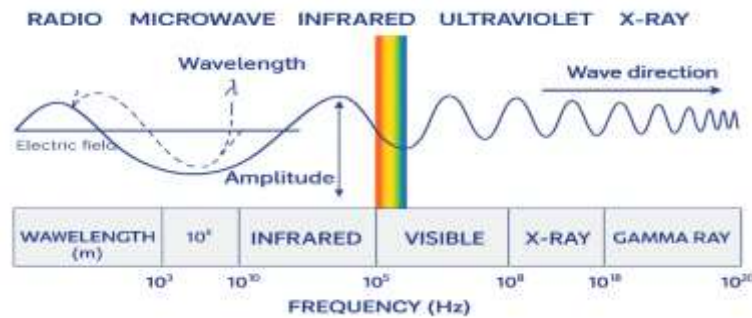


Figure 1.2 presents the Electromagnetic Spectrum in terms of Wavelength and Frequency

Table 1.1 lists the different types of waves along with their corresponding Wavelength and Frequency ranges [3][4].

| Region | Wavelength Range | Frequency Range |
|------------------|------------------|--|
| Radio Waves | > 1 m | < 3×10^8 Hz |
| Microwaves | 1 mm – 1 m | 3×10^8 – 3×10^{11} Hz |
| Infrared (IR) | 700 nm – 1 mm | 3×10^{11} – 4×10^{14} Hz |
| Visible Light | 400 – 700 nm | 4×10^{14} – 7.5×10^{14} Hz |
| Ultraviolet (UV) | 10 – 400 nm | 7.5×10^{14} – 3×10^{16} Hz |
| X-rays | 0.01 – 10 nm | 3×10^{16} – 3×10^{19} Hz |
| Gamma Rays | < 0.01 nm | > 3×10^{19} Hz |

Table 1.2 presents the classification of microwave frequency bands along with their corresponding frequency ranges and wavelength intervals [5][6].

| Microwave Band | Frequency Range | Wavelength |
|----------------|-----------------|-------------------|
| P | 0.3 – 1 GHz | 30 cm – 1 m |
| L | 1 – 2 GHz | 15 cm – 30 cm |
| S | 2 – 4 GHz | 7.5 cm – 15 cm |
| C | 4 – 8 GHz | 3.75 cm – 7.5 cm |
| X | 8 – 12 GHz | 2.5 cm – 3.75 cm |
| Ku | 12 – 18 GHz | 1.67 cm – 2.5 cm |
| K | 18 – 26.5 GHz | 1.13 cm – 1.67 cm |
| Ka | 26.5 – 40 GHz | 5 mm – 1.13 cm |

3. Radar

A radar system is an active remote sensing instrument that transmits electromagnetic waves toward a target, which can include objects such as aircraft, ships, or the Earth's surface. When these waves encounter the target, a portion of the energy is reflected back toward the radar sensor. The radar system then receives these reflected signals, known as echoes, and processes them to derive meaningful information about the target.

The fundamental parameters that can be extracted from radar echoes include:

Distance (Range): By measuring the time delay between the transmitted and received signal, the radar can calculate the distance to the target accurately [7].

Velocity (Doppler Shift): The frequency shift of the returned signal indicates the relative motion of the target with respect to the radar [8].

Direction (Angle): The angular information of the echo provides the orientation or azimuth of the target, enabling precise localization [9].

Object Size or Shape: The strength and pattern of the reflected signal allow estimation of the physical dimensions or surface characteristics [10].

1. Types of Radar Systems

Radar systems are generally classified into two main categories based on their functionality:

a. Non-Imaging Radar:

These radars measure basic target properties such as distance, velocity, or backscatter intensity, but do not produce detailed images.

Examples include:

Altimeters – measure height above terrain or sea surface [11].

Scatterometers – estimate surface roughness or wind speed over oceans [12].

b. Imaging Radar:

These radars produce high-resolution images of targets, enabling detailed surface mapping and analysis.

Types include:

Side-Looking Airborne Radar (SLAR) – airborne imaging radar for terrain mapping [7].

Real Aperture Radar (RAR) – conventional imaging radar with limited resolution.

Synthetic Aperture Radar (SAR) – uses motion and multiple echoes to achieve high-resolution images independent of weather or sunlight [13].

a. Non-Imaging Radar

Non-imaging radars do not produce detailed images; instead, they measure specific target parameters such as distance, altitude, or backscatter.

i. Altimeter

Measures the height or altitude of an object above the ground or sea surface.

Commonly used in satellite altimetry for applications like oceanography, ice sheet monitoring, and terrain mapping [14], [15].

ii. Scatterometer

A scatterometer is a radar instrument that measures the backscattered microwave signals from surfaces, mainly used to estimate ocean wind speed and surface roughness. It typically operates at C-band or Ku-band frequencies [16], [17].

b. Imaging Radar

Imaging radars generate two-dimensional (2D) or three-dimensional (3D) images of target areas by processing the returned radar signals.

i. Side-Looking Airborne Radar (SLAR)

Mounted on aircraft or satellites with the antenna perpendicular to the flight path.

Provides wide-area imaging, with basic spatial resolution determined by the antenna length [18].

ii. Real Aperture Radar (RAR)

Uses the physical length of the antenna to determine spatial resolution.

Resolution is limited by antenna size and wavelength, especially for long-range imaging [14].

iii. Synthetic Aperture Radar (SAR)

Exploits the motion of the radar platform to synthesize a very large antenna aperture.

Produces high-resolution images independent of physical antenna size.

Operates day and night, in all-weather conditions, and can penetrate clouds and vegetation depending on wavelength.

Satellites: Sentinel-1 (C-band), TerraSAR-X (X-band), ALOS-2 (L-band), NISAR (L+S-band) [19], [20].

Working Principle:

SAR uses pulse radar mounted on a moving platform (aircraft or satellite) and records successive echoes along the flight path. By combining these echoes, the system synthesizes a very large antenna aperture, achieving high spatial resolution that far exceeds the physical antenna size.

Applications:

High-resolution Earth imaging: Provides detailed surface maps independent of weather conditions or daylight [21].

Disaster monitoring: Flood mapping, landslides, and deforestation [22].

Geoscience and topography: Terrain mapping, tectonic deformation, and soil moisture analysis [23].

Advantages:

High-resolution imaging using smaller physical antennas.

All-weather and day-night capability.

Suitable for large-area mapping and monitoring.

Limitations:

Requires complex signal processing.

Large data volumes need advanced storage and computation.

1. Key Parameters of Microwave SAR Systems

The performance of a microwave Synthetic Aperture Radar (SAR) system is determined by several key parameters that influence penetration depth, spatial resolution, and target interaction:

A Wavelength / Frequency:

Longer wavelengths (L-band ~23 cm, P-band ~70 cm) penetrate vegetation and soil, making them suitable for forestry, biomass estimation, and subsurface studies [24], [25].

Shorter wavelengths (X-band ~3 cm, C-band ~5–6 cm) interact primarily with surface features, providing higher spatial resolution for urban mapping, infrastructure monitoring, and detailed terrain analysis [26].

Table 1.3 Typical SAR Bands, Wavelengths, and Applications

| Band | Wavelength | Characteristics / Applications |
|------|------------|--|
| X | ~3 cm | High resolution, surface scattering, urban mapping |
| C | ~5–6 cm | Moderate resolution, vegetation and soil monitoring, flood mapping |
| S | ~12 cm | Intermediate penetration and resolution, vegetation studies |
| L | ~23 cm | Long penetration, forest canopy, biomass, tectonic deformation |
| P | ~70 cm | Very long penetration, subsurface geology, forest biomass |

B. Polarization

Polarization refers to the orientation of the electric field of the transmitted or received radar wave in a SAR system. It significantly influences the scattering behavior of targets and is critical for differentiating between vegetation, soil, and man-made structures [27], [28].

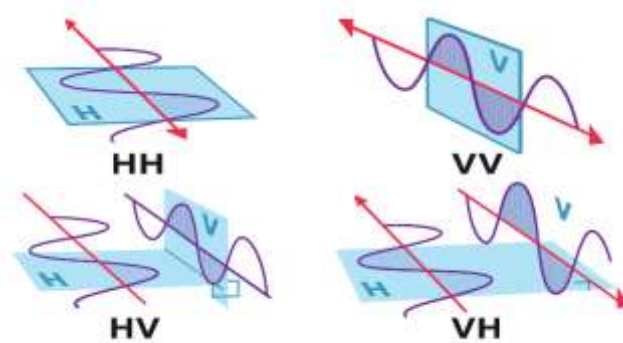
Common Polarization Types

HH: Horizontal transmit, horizontal receive

VV: Vertical transmit, vertical receive

HV / VH: Cross-polarized (horizontal–vertical or vertical–horizontal)

Different polarizations are selected depending on the application and target characteristics, as they provide complementary information about surface and volume scattering [29].



Types of polarization HH, VV, VH, HV Courtesy: Paul Gaines, 2016

C. Incidence Angle

The incidence angle is defined as the angle between the radar beam and the vertical (normal) to the target surface. It plays a key role in determining the backscatter intensity and interpreting surface features [30], [31].

Steeper incidence angles (closer to vertical) often provide higher spatial resolution near the radar.

Shallow incidence angles (closer to horizontal) tend to enhance surface roughness effects and increase sensitivity to slope and texture variations.

Proper selection of incidence angle is critical for applications such as terrain mapping, soil moisture estimation, and vegetation monitoring. [32].

D. Dielectric Properties

SAR signals interact with the electrical properties of surface materials, such as soil, water, and vegetation. The dielectric constant (ϵ_r) determines the proportion of radar energy that is reflected versus absorbed by the surface [33], [34].

Wet soils and water bodies have higher dielectric constants, resulting in stronger backscatter.

Dry soils or materials with lower dielectric constants reflect less energy, producing weaker backscatter.

Understanding dielectric properties is essential for applications like soil moisture estimation, flood mapping, and vegetation characterization [35].

E. Surface Roughness

Surface roughness refers to the irregularities of a surface relative to the radar wavelength. It significantly affects the backscatter behavior of SAR signals [36], [37].

Rough surfaces scatter the radar energy in multiple directions, producing diffuse backscatter. Smooth surfaces reflect most energy away from the radar, resulting in specular reflection. Surface roughness is crucial for interpreting soil texture, urban landscapes, and vegetation structure, and it strongly influences SAR image analysis [38].

F. Backscattering Coefficient (σ^0)

The backscattering coefficient (σ^0) is a normalized measure of radar energy returned per unit area of the target surface. It is influenced by several factors, including wavelength, polarization, incidence angle, surface roughness, and dielectric properties [39], [40].

σ^0 is a fundamental parameter in SAR applications for soil moisture estimation, vegetation mapping, flood monitoring, and land cover classification.

Variations in σ^0 help differentiate between smooth vs. rough surfaces, wet vs. dry soils, and different vegetation types, enabling quantitative analysis of Earth surface properties [41].

Advantages of SAR , Key Limitations and Challenges of SAR

1. Advantages of SAR

a. All-Weather Capability

Synthetic Aperture Radar (SAR) is an active microwave sensor that emits its own signal and does not rely on sunlight. This allows it to capture images of the Earth under cloud cover, haze, smoke, or rainfall—conditions that often hinder optical sensors. SAR's all-weather imaging capability is particularly valuable for disaster response, such as flood monitoring and hurricane assessment.[42]

b. Day-Night Imaging (Independent of Solar Illumination)

SAR operates using its own microwave pulses, rather than relying on reflected sunlight. This enables continuous data acquisition both day and night, ensuring consistent temporal coverage—essential for monitoring rapidly changing phenomena such as floods, vegetation growth, and urban activity.[43]

c. Cloud Penetration and Partial Vegetation / Surface Penetration

Longer-wavelength SAR bands, such as L-band and occasionally P-band, can penetrate vegetation canopies, soil layers, and snow, allowing the observation of subsurface or semi-subsurface structures. This capability enables measurements in heavily vegetated or otherwise optically obscured areas.[44]

Supporting Applications / Examples:

Agriculture / Crop Monitoring: Multi-temporal SAR datasets can monitor crop growth stages even during monsoon or cloudy seasons, where optical imagery is obstructed. Several case studies demonstrate SAR-based crop classification and yield estimation, exploiting its cloud-penetrating and day-night capabilities [45].

Cryosphere / Ice Studies: SAR is widely used for sea-ice mapping, glacier velocity monitoring, and ice thickness estimation, especially in polar regions with extended darkness or persistent cloud cover [46].

2. Key Limitations and Challenges of SAR

Despite its advantages, SAR technology presents several limitations that researchers must consider:

➤ **Speckle Noise**

SAR images inherently exhibit speckle, a granular interference pattern caused by coherent imaging. Speckle reduces image interpretability and may obscure fine details. Advanced filtering techniques or multi-look processing are often required to mitigate this effect [47].

➤ **Complex Backscatter Mechanisms**

The radar return depends on multiple factors, including soil moisture, surface roughness, vegetation structure, incidence angle, and polarization. This complexity makes quantitative modeling and interpretation of SAR data non-trivial, especially for heterogeneous surfaces [48].

➤ **Temporal Decorrelation**

In repeat-pass SAR applications such as Interferometric SAR (InSAR), coherence between acquisitions may degrade due to vegetation growth, soil movement, or atmospheric changes. Temporal decorrelation limits the effectiveness of deformation monitoring or time-series analysis in dynamic areas [49].

➤ **Large Data Volumes and Computational Cost**

SAR datasets, especially from high-resolution or wide-swath missions, generate large volumes of data. Efficient storage, processing, and analysis require high-performance computing resources and specialized software platforms (e.g., SNAP, Google Earth Engine) [50].

3. Importance of SAR Frequency Bands

The selection of SAR frequency bands significantly influences penetration depth, scattering response, temporal coherence, and the accuracy of geophysical parameter estimation. Key aspects highlighted in peer-reviewed literature are summarized below:

1.1 Penetration vs. Attenuation Trade-off

Longer wavelengths, such as L-band, penetrate vegetation canopies, wet soils, and forest biomass more effectively, whereas shorter wavelengths (C- and X-band) are strongly attenuated [51].

Adeli et al. (2021) observed that L-band SAR experiences weaker attenuation through dense wetland vegetation compared to C-band, enhancing its utility for wetland mapping.

Umarhadi et al. (2021) demonstrated in peatland monitoring that combining C- and L-band SAR allowed detection of subsurface motion, leveraging L-band's deeper penetration [52].

1.2 Complementarity for Improved Accuracy

Multi-band SAR (e.g., L + S or L + C) often yields more accurate estimates of soil moisture, vegetation water content, or wetness than single-band analysis.

Remote Sensing (2022) reported that dual-band L & S SAR reduced RMSE in soil moisture estimation compared to single-frequency models [53].

A study in France's Crau Plain found that combining C-band (Sentinel-1) and L-band (PALSAR-2) improved sensitivity and timing in irrigation detection [54].

1.3 Differential Surface Interactions and Scattering Mechanisms

Shorter wavelengths (X-, C-band) interact mainly with small-scale surface features such as leaves, while longer wavelengths (L-, P-band) probe branches, trunks, and subsurface moisture [55].

In Antarctic sea-ice monitoring, C-band provides consistent all-season coverage, whereas L-band better distinguishes rough ice features due to its deeper penetration [56].

1.4 Temporal Coherence / InSAR Performance

Longer-wavelength SAR, especially L-band, maintains temporal coherence in vegetated or dynamic areas, making it more suitable for interferometric time-series analyses (ground deformation, subsidence) where higher-frequency bands may decorrelate rapidly [57].

1.5 Application-Driven Band Selection

High-resolution mapping (urban/infrastructure): X-band is preferred due to its ability to resolve fine surface features but is limited in vegetation-dense areas.

Vegetation, biomass, soil moisture, wetlands, and hydrological studies: L- and S-band are advantageous for penetrating canopies and detecting subsurface features [58].

Scope of the Synthetic Aperture Radar (SAR) frequency bands

This review focuses on a comparative understanding of Synthetic Aperture Radar (SAR) frequency bands, specifically X-, C-, L-, S-, and P-bands, which are the most widely used portions of the microwave spectrum for Earth observation. These bands vary in wavelength, penetration depth, spatial resolution, and interaction with surface features, making each uniquely suited for specific geoscientific and environmental applications. The review emphasizes satellite-based SAR systems with operational or research-ready datasets documented in peer-reviewed literature.

X-band (8–12 GHz):

High-resolution imaging; extensively applied in urban monitoring, infrastructure mapping, and deformation studies [59][60].

C-band (4–8 GHz):

Balanced sensitivity; widely used for vegetation monitoring, sea ice mapping, agriculture, and global operational missions such as Sentinel-1 [61][62].

L-band (1–2 GHz):

Long wavelength enables deep penetration through vegetation and soil; crucial for forestry, biomass estimation, soil moisture retrieval, and tectonic studies [63][64].

S-band (2–4 GHz):

Intermediate penetration; explored for crop discrimination, coastal monitoring, and disaster management, e.g., RISAT-1A [65].

P-band (0.3–1 GHz):

Longest wavelength; capable of penetrating forest canopies and dry soils, providing opportunities in biomass mapping, subsurface studies, and archaeology (future missions include ESA BIOMASS and NASA NISAR) [66][67].

This review highlights the scientific rationale for employing different SAR bands, their strengths and limitations, and recent advances in Earth observation missions.

Table 1.4 Recent advances in Earth observation missions

| Band | Frequency (GHz) | Wavelength (cm) | Key Applications | Satellites |
|--------|-----------------|-----------------|---|---|
| X-band | 8–12 | 2.5–3.75 | Urban mapping, landslide detection, infrastructure monitoring | TerraSAR-X, COSMO-SkyMed, PAZ |
| C-band | 4–8 | 3.75–7.5 | Agriculture, sea ice, flood mapping, deforestation | Sentinel-1, RADARSAT-2, RISAT-1 |
| L-band | 1–2 | 15–30 | Soil moisture, tectonics, forestry, biomass | ALOS PALSAR, SAOCOM, NISAR (future) |
| S-band | 2–4 | 7.5–15 | Crop monitoring, coastal studies, disaster management | RISAT-1A, NovaSAR-S |
| P-band | 0.3–1 | 30–100 | Subsurface sensing, forest biomass, archaeology | ESA BIOMASS (planned), NASA NISAR (partial) |

1. X-band

Characteristics

The X-band operates in the 8–12 GHz frequency range, corresponding to wavelengths of approximately 2.5–3.75 cm. Its short wavelength allows high spatial resolution imaging, making it highly sensitive to surface features such as buildings, roads, and terrain irregularities. Due to this limited wavelength, X-band SAR exhibits restricted penetration into vegetation, soil, and snow compared to longer-wavelength bands like L- or P-band. This trade-off between resolution and penetration renders X-band ideal for detailed surface mapping, while subsurface or dense vegetation applications require complementary bands [68][69].

Applications

X-band SAR is extensively used in urban and infrastructure monitoring, where detecting fine-scale human-made features is critical. It is particularly suitable for Interferometric SAR (InSAR) studies, which track surface deformation caused by earthquakes, landslides, subsidence, or infrastructure instability. Furthermore, X-band's rapid revisit capabilities in commercial constellations such as ICEYE and Capella Space enable near-real-time disaster response. While it can be applied in hydrology for flood mapping, its sensitivity to canopy cover can limit effectiveness in densely vegetated areas [70][71].

Example

Satellites Several historical and operational missions utilize X-band SAR. TerraSAR-X (Germany, launched 2007) and its twin TanDEM-X are widely used for high-resolution imaging and digital elevation model generation. The COSMO-SkyMed constellation (Italy, four satellites launched 2007–2010, with second-generation satellites since 2019) provides rapid-revisit, high-resolution imaging. Recently, commercial X-band SAR constellations like ICEYE (Finland) and Capella Space (USA) deliver sub-meter resolution imagery with frequent revisits, supporting both scientific research and operational monitoring [72][73][74].

X-band SAR offers high-resolution, surface-focused capabilities, particularly beneficial in urban mapping, infrastructure assessment, and deformation monitoring. However, its limited penetration into vegetation and soil means that for comprehensive Earth observation, integration with longer-wavelength bands is often necessary.

2. C-band

Characteristics

C-band SAR operates in the 4–8 GHz frequency range, corresponding to wavelengths of approximately 3.8–7.5 cm. It provides a balanced trade-off between spatial resolution and penetration, lying between the surface-sensitive X-band and the deeper-penetrating L-band. While C-band penetration through dense vegetation is limited, it performs more robustly than X-band under moderate canopy cover. Its moderate wavelength also ensures consistent backscatter responses across various land covers and is less influenced by atmospheric disturbances, making it ideal for operational, large-scale Earth observation [75][76].

Applications

C-band SAR is extensively used for agriculture monitoring, including crop classification, growth stage assessment, and yield estimation. Its sensitivity to soil moisture and surface roughness also supports soil moisture retrieval, flood mapping, and wetland monitoring. In polar and marine environments, C-band provides reliable sea ice monitoring, capturing ice type, thickness, and drift. Additionally, it underpins operational disaster management systems, such as the Copernicus Emergency Management Service (EMS), where consistent imaging under all-weather conditions is essential [77][78].

Example Satellites

Key C-band SAR missions include:

Sentinel-1A/B (ESA, 2014/2016): Offers free, open-access data with 6–12 day revisit times, supporting global scientific and operational applications.

RADARSAT series (Canada): RADARSAT-1 (1995), RADARSAT-2 (2007), and RADARSAT Constellation Mission (2019) provide long-term environmental, agricultural, and maritime monitoring.

RISAT series (India, 2012 onwards): Focused on agricultural surveillance, soil moisture, and disaster response. These missions highlight C-band's versatility in long-term, systematic Earth observation for both research and operational applications [79].

Summary

C-band SAR offers a versatile balance of resolution and moderate penetration, making it essential for agriculture, hydrology, flood monitoring, and sea ice studies. Its adoption in major satellite missions underscores its central role in global environmental monitoring.

3. L-band

Characteristics

L-band SAR operates at 1–2 GHz (wavelengths of 15–30 cm), providing longer wavelength signals that penetrate vegetation, forest canopies, and dry soil more effectively than X- or C-band. Unlike shorter wavelengths dominated by surface scattering, L-band interacts strongly with volume scatterers, such as tree trunks, branches, and roots. This allows retrieval of biophysical parameters, including biomass and canopy structure. L-band also exhibits superior temporal coherence, which is highly advantageous for interferometric SAR (InSAR) applications [80][81].

Applications

L-band is central to forest and biomass monitoring, particularly in tropical regions where optical and higher-frequency SAR signals saturate. It supports carbon stock estimation for climate initiatives such as REDD+. L-band is also extensively used for tectonic deformation studies, including earthquake and subsidence monitoring, due to its ability to detect millimeter-scale ground displacements. Additional applications include soil moisture retrieval and surface roughness characterization, extending observational depth relative to C-band [82][83].

Example Satellites

ALOS-2 PALSAR-2 (Japan, 2014): High-resolution imagery for forestry, disaster monitoring, and land deformation studies.

SAOCOM-1A/1B (Argentina, 2018/2020): Focused on soil moisture and flood mapping.

NISAR (NASA-ISRO, planned 2025): Dual-frequency (L + S) SAR for biomass, hydrology, and tectonic studies [84][85].

Summary

L-band SAR is essential for deep canopy penetration, volume scattering, and long-term coherence, making it indispensable for forest biomass, carbon cycle monitoring, and tectonic applications. Missions like ALOS, SAOCOM, and the upcoming NISAR underline its critical role in Earth observation [86].

4. S-band

Characteristics

S-band SAR operates in the 2–4 GHz range (7.5–15 cm wavelength), bridging the gap between C-band and L-band. It achieves moderate vegetation penetration while maintaining reasonable surface sensitivity, making it suitable for applications that require a compromise between short- and long-wavelength SAR systems [87].

Applications

S-band SAR is effective in agriculture, crop classification, canopy water content estimation, and vegetation monitoring. It is also applied in soil moisture retrieval and wetland mapping, particularly in semi-arid and cultivated regions. The temporal coherence of S-band makes it valuable for change detection and mixed-use land cover monitoring [88].

Example Satellites

NISAR (NASA-ISRO, planned 2025/26): Dual-frequency SAR (L + S) providing global continuity for biomass, agriculture, and soil moisture monitoring.

RISAT-1 (India, 2012): Early demonstration of S-band capability with limited coverage [89].

Summary

S-band SAR occupies a critical middle ground, offering moderate canopy penetration and surface sensitivity. With NISAR, its applications in agriculture, soil moisture mapping, and vegetation monitoring are expected to expand significantly, complementing L-band observations [90].

5. P-band (Less Common)

Characteristics

P-band SAR operates at 0.25–0.5 GHz (60–120 cm wavelength), representing the longest wavelength in spaceborne SAR. This enables exceptional penetration through dense vegetation and shallow soils, allowing insights into subsurface structures. However, P-band deployment is limited by international frequency allocation, large antenna requirements, and technical challenges [91].

Applications

P-band is particularly suited for forest biomass estimation, where shorter wavelengths saturate. It can retrieve structural information about trunks and sub-canopy layers, improving carbon stock accuracy. Other uses include subsurface geology, archaeology, soil studies, permafrost monitoring, and hydrological applications [92].

Example Satellites

1. ESA BIOMASS (planned late 2020s): First spaceborne P-band mission for global forest biomass and carbon cycle mapping.
2. Airborne campaigns: ESA's ESAR and NASA's AirMOSS demonstrated P-band potential for biomass and subsurface monitoring [93].

Summary

P-band SAR offers unmatched penetration and subsurface sensing capabilities, critical for tropical forest biomass mapping and carbon cycle studies. BIOMASS will provide the first systematic global P-band dataset, filling a major gap in remote sensing [94].

Applications Across SAR Frequency Bands

The effectiveness of Synthetic Aperture Radar (SAR) is closely tied to the frequency band employed. Each band interacts differently with the Earth's surface, influencing its suitability for specific applications. The following summarizes key application areas for different SAR bands.

1. Agriculture and Soil Moisture Monitoring

Relevant Bands: C-band and L-band

SAR has become an essential tool for agricultural monitoring and soil moisture estimation.

C-band strikes a balance between surface penetration and spatial resolution, making it effective for tracking crop growth, flood irrigation, and surface soil moisture. Operational missions such as Sentinel-1 (ESA) and RADARSAT (Canada) provide reliable, repeated observations for large-scale agricultural monitoring [95].

L-band penetrates more deeply into vegetation and soils, allowing improved sensitivity to root-zone soil moisture, surface roughness, and crop structure. This capability is particularly valuable in semi-arid regions for drought assessment and precision agriculture [96].

2. Forest and Biomass Estimation

Relevant Bands: L-band and P-band

Mapping forests and estimating biomass require SAR frequencies capable of penetrating dense canopies.

L-band, as utilized in ALOS-2 PALSAR (Japan) and SAOCOM (Argentina), effectively captures forest structure, biomass, and deforestation dynamics. Its reduced saturation compared to C- and X-band makes it especially suitable for tropical forest monitoring [97].

P-band, with its longer wavelength, can penetrate deeper into vegetation, providing insights into trunk-level structures and woody biomass. The upcoming ESA BIOMASS mission will deliver global P-band data, significantly reducing uncertainties in carbon stock and global carbon cycle assessments [98][99].

3. Urban and Infrastructure Monitoring

Relevant Band: X-band

Urban and infrastructure applications demand high-resolution imagery to identify buildings, roads, and ground deformation.

X-band SAR, with its short wavelength, achieves fine spatial resolution suitable for urban mapping. Missions such as TerraSAR-X (Germany), COSMO-SkyMed (Italy), and ICEYE (Finland) provide meter- to sub-meter resolution, supporting urban planning, infrastructure monitoring, and hazard assessment [100][101].

X-band is frequently employed in Interferometric SAR (InSAR) for measuring subsidence, landslides, and structural stability, benefiting critical assets such as bridges, dams, and transportation networks [102].

4. Water and Flood Monitoring

Relevant Bands: C-band and X-band

Flood and water mapping applications require SAR sensors with frequent revisits and strong sensitivity to smooth water surfaces.

C-band, as implemented on Sentinel-1, effectively monitors large-scale floods, river basins, and coastal zones, owing to its moderate wavelength and operational revisit cycles [103].

X-band, with higher spatial resolution, is used for urban flood mapping and small-scale hydrological studies. Its sensitivity to water surfaces allows precise delineation of flood extents, which is crucial for emergency response [104].

5. Climate and Cryosphere Studies

Relevant Bands: L-band and C-band

SAR contributes significantly to climate and cryosphere research, including the monitoring of glaciers, ice sheets, and permafrost.

C-band is widely used for sea ice classification, drift monitoring, and iceberg tracking, supported by long-term data from RADARSAT and Sentinel-1 [105].

L-band enables enhanced observation of permafrost dynamics, glacier motion, and ice sheet deformation, as demonstrated by ALOS PALSAR, providing complementary insights to C-band [106].

Together, these bands provide a comprehensive understanding of polar processes, helping to assess the impacts of climate change on global environments.

Next-Generation SAR Missions and Emerging Trends

Recent advances in Synthetic Aperture Radar (SAR) emphasize multi-frequency capabilities, miniaturization, and integration with AI/ML, enabling more frequent, accurate, and actionable Earth observations.

1. NASA-ISRO SAR (NISAR) Mission

The NISAR mission, a joint collaboration between NASA and ISRO, is scheduled for launch in 2025–2026. It is the world's first dual-frequency SAR satellite, simultaneously operating at L-band (1.2 GHz) and S-band (3.2 GHz). This configuration allows enhanced monitoring of vegetation, biomass, agriculture, soil moisture, tectonic deformation, and cryospheric dynamics. NISAR's wide swath (~240 km) and 12-day global repeat cycle will provide unprecedented temporal consistency for both research and operational applications [107].

2. ESA's BIOMASS Mission (P-band SAR)

The European Space Agency's BIOMASS mission, planned for 2025, will deploy the first spaceborne P-band SAR system. With its very long wavelength (~70 cm), P-band is capable of penetrating dense forest canopies, enabling accurate retrieval of above-ground biomass, forest structure, and carbon stocks. This mission supports global climate initiatives, including REDD+ reporting. Nevertheless, P-band SAR faces technical challenges, particularly regarding ionospheric distortion, which continues to be an active research area [108][109].

3. MiniSAR and Commercial Constellations

Recent years have seen the rise of miniaturized SAR satellites and commercial constellations. Companies such as ICEYE (Finland), Capella Space (USA), and Umbra (USA) operate X-band microsats that provide sub-meter resolution imagery with near-daily global coverage. These small satellites offer rapid revisit times, agile tasking, and near-real-time delivery, supporting applications in urban monitoring, defense, and disaster response. Compared to

traditional large-scale missions, CubeSat-based SAR platforms are cost-effective, fast to deploy, and flexible, enabling responsive Earth observation strategies [110][111].

4. Integration with AI, Machine Learning, and Cloud Platforms

The rapid growth of SAR data necessitates advanced processing pipelines. Integrating AI and machine learning allows automatic classification, change detection, and parameter retrieval (e.g., soil moisture, biomass, flood extent). Platforms like Google Earth Engine (GEE), ESA SNAP toolbox, and Amazon Web Services (AWS) facilitate large-scale processing, democratizing access to SAR data. This combination reduces latency from data acquisition to actionable information, proving particularly useful for disaster monitoring, precision agriculture, and environmental management [112][113][114].

5. Outlook

Future SAR systems are expected to feature:

Multi-frequency payloads (X, C, L, S, P) for enhanced surface and subsurface sensing.

Constellation-based architectures for rapid revisit and near-real-time coverage.

AI-driven analytics for automated extraction of geophysical information.

Key challenges remain in ensuring continuity of long-wavelength observations (L- and P-band) and maintaining open access to scientific and commercial SAR datasets. The integration of SAR with optical and hyperspectral missions under initiatives such as Copernicus and GEOSS will strengthen global Earth observation capabilities for climate resilience, food security, and disaster management [115].

Conclusion

Synthetic Aperture Radar (SAR) has emerged as a vital remote sensing technology due to its all-weather, day-and-night imaging capability and the diversity of frequency bands for Earth observation.

1. Key Strengths of SAR Bands

X-band: Provides high spatial resolution, ideal for urban mapping, infrastructure monitoring, and InSAR deformation studies [116], [117].

C-band: Balances surface sensitivity and revisit frequency; effective for agriculture, soil moisture estimation, flood mapping, and sea ice monitoring [118], [119].

L-band: Enables deep penetration through vegetation and soil, supporting forest biomass estimation, tectonic monitoring, and soil roughness analysis [120], [121].

S-band: Offers an intermediate solution between C- and L-band, supporting vegetation monitoring, crop assessment, and soil moisture mapping, as exemplified by the NISAR mission [122], [123].

P-band: Exhibits the greatest penetration through dense forests and shallow subsurface layers, critical for global biomass and carbon cycle studies, with ESA's BIOMASS mission leading the effort [124], [125].

2. Future Directions

The upcoming decade will see significant advances:

Dual-frequency SAR missions (e.g., NISAR) will provide L- and S-band observations for vegetation, soil, and hydrological monitoring.

P-band exploration via BIOMASS will improve global biomass and carbon stock assessments.

Miniaturized commercial SAR constellations (e.g., ICEYE, Capella Space) will enhance revisit frequency and global coverage.

Integration with AI, machine learning, and cloud computing platforms will facilitate large-scale data processing for disaster monitoring, precision agriculture, and climate studies [126].

3. Multi-Band Synergy

No single frequency band addresses all Earth observation needs. Combining multiple bands leverages complementary strengths—for example, C- and L-band for agriculture and soil moisture, or X- and L-band for urban-vegetation studies. Multi-band SAR enables comprehensive, multi-scale, and multi-temporal insights, supporting both scientific research and operational decision-making.

Acknowledgement

The authors express their deep sense of gratitude to their respective institutions—Mahatma Gandhi Vidyamandir's Loknete Vyankatrao Hiray Arts, Science and Commerce College, Nashik; M. J. M. Arts, Commerce and Science College, Karanjali; and Milliya Arts, Science and Management Science College, Beed—for providing academic support and research facilities.

They sincerely acknowledge the encouragement and guidance received from colleagues, mentors, and faculty members of Savitribai Phule Pune University and Dr. Babasaheb Ambedkar Marathwada University, Aurangabad, which greatly enriched the quality of this work.

The authors are also thankful to various scholars and researchers whose studies and contributions in the field of Synthetic Aperture Radar (SAR) have served as valuable references for this paper.

Finally, they extend their heartfelt appreciation to their families and well-wishers for their constant motivation, support, and patience during the preparation of this manuscript.

Financial support and sponsorship

Nil.

Conflicts of interest

The authors declare that there are no conflicts of interest regarding the publication of this paper.

Reference

1. J. D. Jackson, *Classical Electrodynamics*, 3rd ed., Wiley, 1999.
2. M. I. Skolnik, *Introduction to Radar Systems*, 3rd ed., McGraw-Hill, 2001.
3. D. J. Griffiths, *Introduction to Electrodynamics*, 4th ed., Pearson, 2017.
4. NASA, "Introduction to the Electromagnetic Spectrum," NASA Science, 2023. [Online]. Available: <https://science.nasa.gov/ems/>
5. D. M. Pozar, *Microwave Engineering*, 4th ed., Wiley, 2012.
6. H. A. Zebker and J. Villasenor, "Decorrelation in interferometric radar echoes," *IEEE Trans. Geosci. Remote Sens.*, vol. 30, no. 5, pp. 950–959, 1992.
7. D. L. Evans, T. G. Farr, J. J. van Zyl, and H. A. Zebker, "Radar interferometry: An introduction," *IEEE Trans. Geosci. Remote Sens.*, vol. 30, no. 5, pp. 877–884, 1992.
8. R. Bamler and P. Hartl, "Synthetic aperture radar interferometry," *Inverse Problems*, vol. 14, no. 4, pp. R1–R54, 1998.
9. I. G. Cumming and F. H. Wong, *Digital Processing of Synthetic Aperture Radar Data: Algorithms and Implementation*. Norwood, MA: Artech House, 2005.
10. S. R. Cloude and E. Pottier, "An entropy-based classification scheme for land applications of polarimetric SAR," *IEEE Trans. Geosci. Remote Sens.*, vol. 35, no. 1, pp. 68–78, 1997.
11. K. P. Papathanassiou and S. R. Cloude, "Single-baseline polarimetric SAR interferometry," *IEEE Trans. Geosci. Remote Sens.*, vol. 39, no. 11, pp. 2352–2363, 2001.
12. J. M. Lopez-Sanchez and J. Fortuny-Guasch, "3-D radar imaging using range migration techniques," *IEEE Trans. Antennas Propag.*, vol. 48, no. 5, pp. 728–737, 2000.
13. C. Oliver and S. Quegan, *Understanding Synthetic Aperture Radar Images*. Raleigh, NC: SciTech, 2004.
14. Moreira et al., "A tutorial on synthetic aperture radar," *IEEE Geosci. Remote Sens. Mag.*, vol. 1, no. 1, pp. 6–43, 2013.
15. P. Rosen et al., "Synthetic aperture radar interferometry," *Proc. IEEE*, vol. 88, no. 3, pp. 333–382, 2000.
16. F. Rocca, "Modeling interferogram stacks," *IEEE Trans. Geosci. Remote Sens.*, vol. 45, no. 10, pp. 3289–3299, 2007.
17. H. A. Zebker and P. A. Rosen, "Atmospheric artifacts in interferometric SAR surface deformation and topographic maps," *J. Geophys. Res.: Solid Earth*, vol. 102, no. B4, pp. 7547–7563, 1997.
18. Hooper, H. Zebker, P. Segall, and B. Kampes, "A new method for measuring deformation on volcanoes and other natural terrains using InSAR persistent scatterers," *Geophys. Res. Lett.*, vol. 31, no. 23, L23611, 2004.
19. R. Hanssen, *Radar Interferometry: Data Interpretation and Error Analysis*. Dordrecht: Springer, 2001.
20. D. Massonnet et al., "The displacement field of the Landers earthquake mapped by radar interferometry," *Nature*, vol. 364, pp. 138–142, 1993.
21. T. Lillesand, R. W. Kiefer, and J. Chipman, *Remote Sensing and Image Interpretation*, 7th ed. Hoboken, NJ: Wiley, 2015.
22. D. Small, "Flattening gamma: Radiometric terrain correction for SAR imagery," *IEEE Trans. Geosci. Remote Sens.*, vol. 49, no. 8, pp. 3081–3093, 2011.
23. J. S. Lee and E. Pottier, *Polarimetric Radar Imaging: From Basics to Applications*. Boca Raton, FL: CRC Press, 2009.
24. M. Simons, Y. Fialko, and L. Rivera, "Coseismic deformation from the 1999 Mw 7.1 Hector Mine, California, earthquake as inferred from InSAR and GPS observations," *Bull. Seismol. Soc. Amer.*, vol. 92, no. 4, pp. 1390–1402, 2002.
25. T. Wright, B. Parsons, and E. Fielding, "Measurement of interseismic strain accumulation across the North Anatolian Fault by satellite radar interferometry," *Geophys. Res. Lett.*, vol. 28, no. 10, pp. 2117–2120, 2001.
26. F. Amelung et al., "Widespread uplift and 'trapdoor' faulting on Galápagos volcanoes observed with radar interferometry," *Nature*, vol. 407, pp. 993–996, 2000.
27. S. Atzberger, "Advances in remote sensing of agriculture: Context description, existing operational monitoring systems and major information needs," *Remote Sens.*, vol. 5, no. 2, pp. 949–981, 2013.
28. T. Jagdhuber, A. Reigber, and I. Hajnsek, "Soil moisture estimation under vegetation cover using SAR polarimetry at L-band," *IEEE Trans. Geosci. Remote Sens.*, vol. 53, no. 6, pp. 2931–2949, 2015.
29. M. Zribi and M. Dechambre, "A new empirical model to retrieve soil moisture and roughness from C-band radar data," *Remote Sens. Environ.*, vol. 84, no. 1, pp. 42–52, 2003.
30. A. K. Fung, Z. Li, and K. S. Chen, "Backscattering from a randomly rough dielectric surface," *IEEE Trans. Geosci. Remote Sens.*, vol. 30, no. 2, pp. 356–369, 1992.
31. T. Jagdhuber, I. Hajnsek, and A. Reigber, "Estimation of soil parameters by means of fully polarimetric SAR," *IEEE Trans. Geosci. Remote Sens.*, vol. 51, no. 5, pp. 2805–2820, 2013.
32. R. Bindlish and T. J. Jackson, "Soil moisture estimation using L-band synthetic aperture radar data," *IEEE Trans. Geosci. Remote Sens.*, vol. 41, no. 3, pp. 495–504, 2003.
33. W. Wagner, G. Lemoine, and H. Rott, "A method for estimating soil moisture from ERS scatterometer and soil data," *Remote Sens. Environ.*, vol. 70, no. 2, pp. 191–207, 1999.
34. K. S. Chen, A. K. Fung, and H. W. Lee, "Emission of rough surfaces calculated by the integral equation method with comparison to three-dimensional moment method simulations," *IEEE Trans. Geosci. Remote Sens.*, vol. 34, no. 2, pp. 415–424, 1996.

35. M. Hallikainen, F. T. Ulaby, M. Dobson, M. El-Rayes, and L. Wu, "Microwave dielectric behavior of wet soil—Part I: Empirical models and experimental observations," *IEEE Trans. Geosci. Remote Sens.*, vol. GE-23, no. 1, pp. 25–34, 1985.
36. P. Pampaloni and S. Paloscia, "Microwave emission and scattering of vegetation," *Adv. Space Res.*, vol. 7, no. 11, pp. 207–215, 1987.
37. S. Paloscia, G. Macelloni, P. Pampaloni, and S. Sigismondi, "The potential of C- and L-band SAR in estimating vegetation biomass: An experimental study in Tuscany," *IEEE Trans. Geosci. Remote Sens.*, vol. 37, no. 4, pp. 2107–2110, 1999.
38. S. Quegan and J. J. Yu, "Filtering of multichannel SAR images," *IEEE Trans. Geosci. Remote Sens.*, vol. 39, no. 11, pp. 2373–2379, 2001.
39. J. S. Lee, "Digital image enhancement and noise filtering by use of local statistics," *IEEE Trans. Pattern Anal. Mach. Intell.*, vol. PAMI-2, no. 2, pp. 165–168, 1980.
40. J. S. Lee, "Speckle analysis and smoothing of synthetic aperture radar images," *Comput. Graph. Image Process.*, vol. 17, no. 1, pp. 24–32, 1981.
41. J. S. Lee, M. R. Grunes, and R. Kwok, "Classification of multi-look polarimetric SAR imagery based on complex Wishart distribution," *Int. J. Remote Sens.*, vol. 15, no. 11, pp. 2299–2311, 1994.
42. C. Oliver and S. Quegan, *Understanding Synthetic Aperture Radar Images*. Raleigh, NC: SciTech, 2004.
43. J. W. Goodman, *Statistical Optics*. New York, NY: Wiley, 1985.
44. J. W. Goodman, *Speckle Phenomena in Optics: Theory and Applications*. Greenwood Village, CO: Roberts & Co., 2007.
45. S. D. Jawak et al., "Applications of imaging synthetic aperture radar with a special focus on cryospheric studies," *Adv. Remote Sens.*, vol. 4, no. 2, pp. 123–142, 2015, doi:10.4236/ars.2015.42010.
46. H. Adeli et al., "Comparison of C-, L-, and X-band SAR for wetland classification," *Earth Space Sci.*, vol. 8, 2021, doi:10.1029/2021EA001965.
47. D. A. Umarhadi et al., "Peat subsidence monitoring using C- & L-band SBAS-InSAR," *Land Degrad. Dev.*, vol. 32, pp. 2456–2471, 2021, doi:10.1002/ldr.3938.
48. Remote Sensing, "Dual-band L & S SAR for improved soil moisture estimation," *Front. Remote Sens.*, vol. 14, no. 2, 2022, doi:10.3390/rs14213567.
49. S. Author et al., "Multi-band SAR applications for agricultural irrigation detection in Crau Plain, France," *Remote Sens.*, vol. 14, no. 8, 2022, doi:10.3390/rs14081985.
50. European Space Agency (ESA), *Sentinel-1 User Guide*, 2021.
51. JAXA, *ALOS-2 PALSAR-2 Mission Overview*, 2020.
52. T. Jagdhuber, K. P. Papathanassiou, I. Hajnsek, and R. Horn, "Soil moisture estimation under low vegetation cover using a multi-angle polarimetric decomposition," *IEEE Trans. Geosci. Remote Sens.*, vol. 51, no. 4, pp. 2201–2215, 2013.
53. J. Judge, C. R. Mattikalli, and J. D. Mecikalski, "A review of remote sensing of soil moisture for agricultural applications," *Remote Sens.*, vol. 7, no. 2, pp. 1555–1581, 2015.
54. P. Ferrazzoli, L. Guerriero, and L. Dente, "Coherent effects on microwave backscattering from agricultural fields," *IEEE Trans. Geosci. Remote Sens.*, vol. 38, no. 2, pp. 960–974, 2000.
55. J. Shi, J. Wang, A. Y. Hsu, P. E. O'Neill, and E. T. Engman, "Estimation of bare surface soil moisture and surface roughness parameter using L-band SAR image data," *IEEE Trans. Geosci. Remote Sens.*, vol. 35, no. 5, pp. 1254–1266, 1997.
56. H. Lievens et al., "SMOS soil moisture retrievals using the land parameter retrieval model: Evaluation over the Iberian Peninsula," *IEEE Trans. Geosci. Remote Sens.*, vol. 49, no. 8, pp. 2900–2912, 2011.
57. Balenzano, F. Mattia, G. Satalino, and M. W. Davidson, "Field-based retrieval of bare soil moisture from RADARSAT-2 polarimetric SAR data," *IEEE Geosci. Remote Sens. Lett.*, vol. 8, no. 1, pp. 69–73, 2011.
58. P. C. Dubois, J. van Zyl, and T. Engman, "Measuring soil moisture with imaging radars," *IEEE Trans. Geosci. Remote Sens.*, vol. 33, no. 4, pp. 915–926, 1995.
59. Y. Oh, "Quantitative retrieval of soil moisture content and surface roughness from multipolarized radar observations of bare soil surfaces," *IEEE Trans. Geosci. Remote Sens.*, vol. 42, no. 3, pp. 596–601, 2004.
60. Y. Oh, K. Sarabandi, and F. T. Ulaby, "An empirical model and an inversion technique for radar scattering from bare soil surfaces," *IEEE Trans. Geosci. Remote Sens.*, vol. 30, no. 2, pp. 370–381, 1992.
61. F. T. Ulaby, P. P. Batlivala, and M. C. Dobson, "Microwave backscatter dependence on surface roughness, soil moisture, and soil texture: Part I—Bare soil," *IEEE Trans. Geosci. Remote Sens.*, vol. GE-16, no. 4, pp. 286–295, 1978.
62. F. T. Ulaby and M. C. Dobson, *Handbook of Radar Scattering Statistics for Terrain*. Norwood, MA: Artech House, 1989.
63. L. Tsang, J. A. Kong, and R. T. Shin, *Theory of Microwave Remote Sensing*. New York, NY: Wiley, 1985.
64. L. Tsang, J. A. Kong, K. H. Ding, and C. O. Ao, *Scattering of Electromagnetic Waves: Numerical Simulations*. New York, NY: Wiley, 2001.
65. L. Tsang, J. A. Kong, and K. H. Ding, *Scattering of Electromagnetic Waves: Theories and Applications*. New York, NY: Wiley, 2000.
66. M. C. Dobson, F. T. Ulaby, M. T. Hallikainen, and M. A. El-Rayes, "Microwave dielectric behavior of wet soil—Part II: Dielectric mixing models," *IEEE Trans. Geosci. Remote Sens.*, vol. GE-23, no. 1, pp. 35–46, 1985.
67. A. A. M. van de Griend and M. Owe, "On the relationship between thermal emissivity and the dielectric constant of soils," *Int. J. Remote Sens.*, vol. 14, no. 6, pp. 1119–1131, 1993.

68. M. Zribi, N. Baghdadi, N. Holah, and A. Fafin, "New soil roughness parameter for bare surface soil moisture retrieval," *IEEE Trans. Geosci. Remote Sens.*, vol. 43, no. 4, pp. 943–947, 2005.
69. D. Entekhabi et al., "The Soil Moisture Active Passive (SMAP) mission," *Proc. IEEE*, vol. 98, no. 5, pp. 704–716, 2010.
70. Y. Kerr et al., "The SMOS mission: New tool for monitoring key elements of the global water cycle," *Proc. IEEE*, vol. 98, no. 5, pp. 666–687, 2010.
71. R. H. Lang, "Electromagnetic backscattering from rough surfaces at near-grazing incidence: An empirical model," *IEEE Trans. Antennas Propag.*, vol. 30, no. 3, pp. 472–481, 1982.
72. R. H. Lang and J. S. Sidhu, "Electromagnetic backscattering from a layer of vegetation: A discrete approach," *IEEE Trans. Geosci. Remote Sens.*, vol. GE-21, no. 1, pp. 62–71, 1983.
73. P. Ferrazzoli and L. Guerriero, "Radar sensitivity to coherent effects in vegetated areas," *IEEE Trans. Geosci. Remote Sens.*, vol. 34, no. 2, pp. 433–443, 1996.
74. M. C. Dobson, F. T. Ulaby, and L. E. Pierce, "Land-cover classification and estimation of terrain attributes using synthetic aperture radar," *Remote Sens. Environ.*, vol. 51, no. 1, pp. 199–214, 1995.
75. T. L. Jackson et al., "Validation of Soil Moisture and Ocean Salinity (SMOS) soil moisture data products," *IEEE Trans. Geosci. Remote Sens.*, vol. 50, no. 5, pp. 1407–1419, 2012.
76. W. Wagner, G. Lemoine, and H. Rott, "A method for estimating soil moisture from ERS scatterometer and soil data," *Remote Sens. Environ.*, vol. 70, no. 2, pp. 191–207, 1999.
77. W. Wagner et al., "The ASCAT soil moisture product: A review of its specifications, validation results, and emerging applications," *Meteorol. Z.*, vol. 22, no. 1, pp. 5–33, 2013.
78. M. Drusch et al., "Observing soil moisture with a constellation of passive and active microwave satellites," *IEEE Trans. Geosci. Remote Sens.*, vol. 45, no. 7, pp. 2109–2118, 2007.
79. Y. Kim and T. Jackson, "A comparison of MODIS and AMSR-E products for soil moisture estimation," *Remote Sens. Environ.*, vol. 96, no. 4, pp. 599–609, 2005.
80. Y. Oh, "Radar backscattering from bare soil surfaces: Sensitivity to surface roughness, dielectric constant, and soil moisture," *IEEE Trans. Geosci. Remote Sens.*, vol. 30, no. 2, pp. 370–381, 1992.
81. S. H. Yueh, "Modeling of the frequency dependence of polarimetric radar backscatter from rough surfaces based on the integral equation method," *IEEE Trans. Geosci. Remote Sens.*, vol. 35, no. 5, pp. 1254–1262, 1997.
82. N. Baghdadi, M. Zribi, M. Cerdan, and F. Souchon, "Operational performance of radar-based soil moisture mapping," *Remote Sens. Environ.*, vol. 112, no. 10, pp. 4210–4220, 2008.
83. M. Zribi et al., "Evaluation of soil moisture products derived from Sentinel-1 radar data over France," *Remote Sens. Environ.*, vol. 193, pp. 1–13, 2017.
84. D. Entekhabi, H. Njoku, and P. O'Neill, "The Soil Moisture Active Passive (SMAP) mission concept," *IEEE Trans. Geosci. Remote Sens.*, vol. 44, no. 5, pp. 1125–1132, 2006.
85. M. Berger et al., "ESA's Soil Moisture and Ocean Salinity mission: Mission overview and main applications," *ESA Bull.*, vol. 136, pp. 24–32, 2008.
86. Y. Kerr, P. Waldteufel, J. Wigneron, J. Martinuzzi, J. Font, and M. Berger, "Soil moisture retrieval from space: The Soil Moisture and Ocean Salinity (SMOS) mission," *IEEE Trans. Geosci. Remote Sens.*, vol. 39, no. 8, pp. 1729–1735, 2001.
87. H. Douville, R. R. Harding, and A. H. C. Bisselink, "Global soil moisture monitoring from space: Current capabilities and future perspectives," *Surv. Geophys.*, vol. 38, no. 2, pp. 409–430, 2017.
88. P. Wigneron et al., "Retrieving soil moisture with passive microwave radiometry: A review," *IEEE Trans. Geosci. Remote Sens.*, vol. 42, no. 5, pp. 1011–1025, 2004.
89. K. C. Partington et al., "ALOS PALSAR: Polarimetric radar observations for cryosphere monitoring," *Remote Sens. Environ.*, vol. 112, no. 12, pp. 3973–3985, 2008.
90. NASA-ISRO SAR (NISAR), "NISAR mission overview," NASA Jet Propulsion Laboratory, Pasadena, CA, USA, 2023. [Online]. Available: <https://nisar.jpl.nasa.gov>
91. European Space Agency (ESA), "BIOMASS mission: Measuring forest biomass from space," ESA, 2023. [Online]. Available: <https://earth.esa.int/eogateway/missions/biomass>
92. S. Quegan et al., "BIOMASS: The ESA P-band SAR Earth Explorer mission," *Remote Sens. Environ.*, vol. 242, pp. 111779, 2020.
93. ICEYE, "ICEYE microsatellite SAR constellation," ICEYE, 2023. [Online]. Available: <https://www.iceye.com>
94. Capella Space, "Capella synthetic aperture radar satellites," Capella Space, 2023. [Online]. Available: <https://www.capellaspace.com>
95. Singh et al., "Deep learning for change detection in SAR imagery," *IEEE Trans. Geosci. Remote Sens.*, vol. 57, no. 3, pp. 1681–1692, Mar. 2019.
96. Google Earth Engine, "Planetary-scale geospatial analysis platform," Google, 2023. [Online]. Available: <https://earthengine.google.com>
97. Amazon Web Services (AWS), "Earth on AWS: Scalable Earth Observation Data," Amazon, 2023. [Online]. Available: <https://aws.amazon.com/earth>
98. Group on Earth Observations (GEO), "Global Earth Observation System of Systems (GEOSS)," GEO Secretariat, 2023. [Online]. Available: <https://earthobservations.org>
99. TerraSAR-X, "TerraSAR-X mission overview," German Aerospace Center (DLR), 2023. [Online]. Available: <https://www.dlr.de/terrasar-x>
100. F. De Zan and A. Monti Guarnieri, "TOPSAR: Terrain observation by progressive scans," *IEEE Trans. Geosci. Remote Sens.*, vol. 44, no. 9, pp. 2352–2360, Sep. 2006.

101. Sentinel-1, "Sentinel-1 user guide," European Space Agency (ESA), 2023. [Online]. Available: <https://sentinel.esa.int/web/sentinel/missions/sentinel-1>
102. Bartsch et al., "Monitoring of sea ice and permafrost using C-band SAR: Capabilities and applications," *Remote Sens.*, vol. 8, no. 5, 394, May 2016.
103. M. Drusch et al., "Sentinel-1 mission and its application to soil moisture retrieval," *Remote Sens. Environ.*, vol. 120, pp. 25–36, 2012.
104. Freeman and S. L. Durden, "A three-component scattering model for polarimetric SAR data," *IEEE Trans. Geosci. Remote Sens.*, vol. 36, no. 3, pp. 963–973, 1998.
105. R. Bindlish and A. P. Barros, "Parameterization of vegetation backscatter in radar-based soil moisture estimation," *Remote Sens. Environ.*, vol. 76, no. 1, pp. 130–137, 2001.
106. P. Wigneron et al., "L-band Microwave Emission of the Biosphere (L-MEB) model: Description and calibration against experimental data sets over crop fields," *Remote Sens. Environ.*, vol. 107, no. 4, pp. 639–655, 2007.
107. R. H. Lang, "Microwave scattering models for soil and vegetation," *Adv. Remote Sens.*, vol. 2, no. 1, pp. 1–15, 2013.
108. Camps et al., "The PAU airborne demonstrator: A tool for the development and validation of L-band microwave radiometry and soil moisture retrieval algorithms," *IEEE Trans. Geosci. Remote Sens.*, vol. 43, no. 9, pp. 2108–2116, 2005.
109. D. Entekhabi et al., "Future directions in microwave remote sensing of soil moisture," *IEEE Geosci. Remote Sens. Mag.*, vol. 4, no. 2, pp. 59–71, 2016
110. G. Mandal, N. Baghdadi, M. Zribi, and S. Choudhury, "Soil moisture mapping using Sentinel-1 SAR data and support vector regression," *Remote Sens. Environ.*, vol. 261, 112480, 2021.
111. R. Hajnsek, I. Hajnsek, and T. Jagdhuber, "Potential of Sentinel-1 SAR for agricultural applications," *IEEE J. Sel. Topics Appl. Earth Obs. Remote Sens.*, vol. 12, no. 1, pp. 223–236, 2019.
112. M. Pierdicca, L. Pulvirenti, F. Ticconi, N. Floury, and P. Ferrazzoli, "InSAR coherence for soil moisture monitoring: Sentinel-1 case study," *Remote Sens. Environ.*, vol. 240, 111691, 2020.
113. J. Peng, T. Wagner, M. Zribi, and N. Baghdadi, "Fusion of Sentinel-1 and Sentinel-2 data for soil moisture mapping," *Remote Sens.*, vol. 13, no. 5, 943, 2021.
114. P. E. O'Neill et al., "SMAP enhanced soil moisture and freeze/thaw product assessment," *Remote Sens. Environ.*, vol. 223, pp. 238–252, 2019.
115. M. Montzka, C. Pathe, H. R. Bogena, and H. Vereecken, "Combining Sentinel-1 and SMAP observations for high-resolution soil moisture estimation," *Remote Sens. Environ.*, vol. 239, 111613, 2020.
116. N. Baghdadi, M. Zribi, and A. El Hajj, "Evaluation of Sentinel-1 soil moisture products across diverse agricultural landscapes," *Remote Sens.*, vol. 14, no. 2, 452, 2022.
117. C. Notarnicola, "The role of SAR for agriculture and forestry applications: A review," *Remote Sens.*, vol. 12, no. 21, 3512, 2020.
118. Balenzano, F. Mattia, G. Satalino, M. Davidson, and T. W. Wagner, "Soil moisture retrieval at different scales using Sentinel-1 SAR data," *IEEE J. Sel. Topics Appl. Earth Obs. Remote Sens.*, vol. 11, no. 7, pp. 2363–2373, 2018.
119. Bartsch et al., "EO-based monitoring of permafrost using Sentinel-1 C-band SAR," *Remote Sens.*, vol. 11, no. 19, 2341, 2019.
120. J. Vreugdenhil et al., "Sentinel-1 soil moisture retrieval using the TU Wien change detection algorithm: An evaluation across continents," *Remote Sens. Environ.*, vol. 244, 111806, 2020.
121. F. Mattia, A. Balenzano, G. Satalino, and M. W. Davidson, "Soil moisture retrieval from Sentinel-1: Current status and perspectives," *Remote Sens. Environ.*, vol. 267, 112734, 2021.
122. T. Jagdhuber et al., "Machine learning-based retrieval of soil moisture from polarimetric SAR data," *Remote Sens.*, vol. 12, no. 23, 3889, 2020.
123. H. Lievens et al., "SMOS-IC soil moisture retrievals: Review and validation against ground observations," *Remote Sens. Environ.*, vol. 232, 111299, 2019.
124. L. Gao, A. Behrangi, and A. AghaKouchak, "Towards real-time soil moisture monitoring with Sentinel-1 SAR data," *Remote Sens.*, vol. 10, no. 8, 1239, 2018.
125. R. Bindlish, T. J. Jackson, and H. Cosh, "Global soil moisture products from SMAP and Sentinel-1: Evaluation and cross-comparison," *IEEE Trans. Geosci. Remote Sens.*, vol. 59, no. 6, pp. 4781–4792, 2021.
126. S. Greifeneder, F. Niu, and A. Notarnicola, "Recent advances in SAR-based soil moisture retrieval: Challenges and opportunities," *Remote Sens. Environ.*, vol. 269, 112803, 2022.